Received: 1 October 2021 | Revised: 15 December 2021 | Accepted: 16 December 2021

DOI: 10.1002/sia.7059

RESEARCH ARTICLE

SURFACE and INTERFACE ANALYSIS WILEY

Quantification of hard X-ray photoelectron spectroscopy: Calculating relative sensitivity factors for 1.5- to 10-keV photons in any instrument geometry

David J. H. Cant[1] | Ben F. Spencer[2] | Wendy R. Flavell[3] | Alexander G. Shard[1]

[1]National Physical Laboratory, Teddington, UK

[2]Henry Royce Institute and the Department of Materials, School of Natural Sciences, The University of Manchester, Manchester, UK

[3]Henry Royce Institute, Photon Science Institute, and Department of Physics and Astronomy, School of Natural Sciences, The University of Manchester, Manchester, UK

Correspondence
David J. H. Cant, National Physical Laboratory, Hampton Road, Teddington, UK.
Email: david.cant@npl.co.uk

Funding information
Henry Royce Institute, Grant/Award Numbers: EP/P025021/1, EP/P025498/1, EP/R00661X/1; UK Department of Business, Energy, and Industrial Strategy, Grant/Award Number: NMS/ST20-21

A method for the rapid determination of theoretical relative sensitivity factors (RSFs) for hard X-ray photoelectron spectroscopy (HAXPES) instruments of any type and photon energy has been developed. We develop empirical functions to describe discrete theoretically calculated values for photoemission cross sections and asymmetry parameters across the photon energy range from 1.5 to 10 keV for all elements from lithium to californium. The formulae describing these parameters, in conjunction with similar practical estimates for inelastic mean free paths, allow the calculation of a full set of theoretical sensitivity factors for a given X-ray photon energy, X-ray polarisation and instrument geometry. We show that the anticipated errors on these RSFs are less than the typical errors generated by extracting X-ray photoelectron spectroscopy (XPS) intensities from the spectra and thus enable adequate quantification for any XPS/HAXPES experiment up to 10 keV. A spreadsheet implementation of this method is provided in the supporting information, along with example RSFs for existing commercial instruments.

KEYWORDS
calibration, HAXPES, photoelectron spectroscopy, sensitivity factors, XPS

1 | INTRODUCTION

X-ray photoelectron spectroscopy (XPS) is a widely used analytical technique in both academic and commercial studies due to its ability to provide quantitative measurements of the relative proportions of chemical species present upon a surface. This capability is due in no small part to the extensive body of work on the development of XPS metrology, calibration and standardisation.[1–8] The vast majority of lab-based XPS instruments use an aluminium anode X-ray source with a monochromator to isolate Al Kα X-rays with a photon energy of 1486.6 eV, which provides an information depth of approximately 5 to 10 nm (dependent on sample material, photoelectron kinetic energy, and electron emission angle). XPS measurement of sample regions deeper than this usually requires either the use of destructive depth profiling, for example, with an ion beam source, or access to beamtime on a hard X-ray photoelectron spectroscopy (HAXPES) end-station at a synchrotron facility, where higher photon energies are available with high intensity. Depth profiling has the disadvantage of being destructive, whereas HAXPES requires access to highly competitive beamtime using instrumentation that is difficult to calibrate to the same accuracy as lab-based equipment.

Recently, several XPS instrument manufacturers have begun supplying lab-based instrumentation possessing higher energy X-ray sources. Although the potential for lab-based higher energy X-ray sources has been understood for some time,[9] the inclusion of such sources on commercially available instruments has been limited until now. This has become feasible partly due to the improvement in X-ray source intensities and partly due to the improved sensitivity of modern analysers. These instruments include the use of silver,[10] chromium[11,12] and liquid-gallium[13,14] based anodes, making use of the Ag Lα (2984.3 eV), Cr Kα (5417 eV) and Ga Kα (9.25 keV) emission lines, respectively. Higher energy instruments afford users potential advantages: the capability to make measurements deeper beneath the sample surface; the additional core levels that may be

accessed (which may have greater sensitivity than using lower binding energy core levels with a lower energy X-ray source and/or may provide alternative peaks when lower binding energy core levels overlap other photoelectron and/or Auger peaks); and their potential for non-destructive depth distribution analysis when used in combination with traditional, lower X-ray energy XPS analysis.[15,16] The latter is particularly of importance when compared with commonly used destructive depth profiling techniques such as sputtering, which bear much greater risk of altering the sample in a way that may produce erroneous spectra, either through damage or preferential removal of material. Specific opportunities include: the ability to measure technologically important materials, where film thicknesses larger than 10 nm are common; discrimination of common interferences, such as the detection of aluminium in copper and alloys of 3d transition metals (in which the important 2p photoelectron peaks overlap the LMM Auger features when using an Al Kα source); and minimising the contribution of the altered surface layer in sputter depth profiling to obtain more accurate chemical analysis.[17] Information from an extended depth into the surface is also obtained by measuring the inelastic background, where HAXPES allows a greater energy range between peaks, allowing measurement of the energy loss function over an extended range of kinetic energy compared with XPS.[14,18–20]

The widespread use of lab-based HAXPES instrumentation is currently in its infancy. In order to ensure its future utility and relevance, it is necessary to employ the same level of careful metrological work that enabled traditional XPS analysis to become the most trusted and widely used surface analysis method.[21] In order to allow quantitative measurements of the amount of material present, two key features of an XPS or HAXPES experiment must be likewise quantified, namely, the intensity/energy response function of the spectrometer and the relative electron intensity emitted from different materials under a given instrumental setup (geometry, photon energy, etc.). The latter is commonly accounted for using relative sensitivity factors (RSFs) for the core levels of each element; these may be obtained by a number of different methods. Arguably, the best option is to determine sensitivity factors experimentally for the specific instrument in question; however, this is an extremely time-consuming and painstaking task that is unreasonable to expect for the average user.[22–24] Reliance on widespread adoption of this method would therefore become a significant bottleneck for robust, comparable HAXPES measurements. Alternatively, the user may rely upon a published database of experimentally determined sensitivity factors, so long as these have been obtained under the appropriate instrument setup and contain values for all the materials the user intends to analyse. Finally, the user may rely upon theoretically calculated sensitivity factors—these can be readily provided for all potential instrument setups but are reliant on the validity of the intensity calibration method. It should be noted that regardless of the method chosen, the quantification obtained using RSFs provides values for the homogeneous-equivalent atomic concentration of the elements and chemical species present. This assumption of homogeneity is open to question, particularly over the significant sampling depths measured in a HAXPES experiment. These values therefore provide an amalgamation of concentration and depth distribution information.

For several HAXPES instruments, databases of sensitivity factors have already been published, including theoretical values for Ag Lα[10] and Ga Kα[14] sources and empirical values for a range of photon energies[25] as determined at a synchrotron light source. Given the range of X-ray source energies now available, it is desirable that sensitivity factors determined using similar methodology should be made available for all instrument setups. In this paper, we describe a method of calculating the most important parameters required for generating a database of sensitivity factors for any given instrumental setup with an excitation source energy between 1.5 and 10 keV. This method consists of a set of empirical formulae and coefficients, determined by fitting to existing databases of theoretically calculated values that are calculated at discrete energies, typically in 1000-eV steps. This method, which is encapsulated in an electronic spreadsheet in the supporting information, allows the user to generate sensitivity factors for any specified instrumental setup without requiring an expert understanding of theory, access to databases or knowledge of the most appropriate interpolation methods. The errors in the calculated values for the modelled parameters are shown to be less than the typical errors involved in the determination of peak intensities from an XPS spectrum,[22] therefore indicating that the generated RSFs allow adequate quantification for any XPS or HAXPES experiment that uses a source energy between 1.5 and 10 keV.

2 | AVERAGE MATRIX RSFS

When performing measurements using XPS, the X-ray photoelectron intensity emitted from the surface for a specific electronic core level, at a specific angle of emission, can be expressed by Equation 1[2]:

$$I_A^\infty \propto J\sigma\lambda TS[1+sF] \quad (1)$$

where J is the photon flux incident on the sample; σ is the total photoionisation cross section for a specific subshell; λ is the inelastic mean-free-path (IMFP[26]) for electrons with a given kinetic energy; T is a function describing the reduction in the observed intensity of electrons emitted with a given kinetic energy due to instrumental losses between emission and detection, known as the transmission function; F is a parameter describing the angular anisotropy of electrons emitted from a given subshell; S is a factor less than 1, which depends upon the material and the emission angle and describes the reduction in the observed intensity of electrons emitted with a given kinetic energy due to elastic scattering effects; and s is a factor less than 1, which depends upon the material and the emission angle and describes the change in angular distribution of electrons emitted at a given kinetic energy due to elastic scattering effects.

For the purposes of performing quantification of peak intensities within a spectrum, the typical user is concerned only with the relative intensities of each peak, thus the photon flux (which should be constant for a given measurement) can be ignored. The instrumental

energy-dependent transmission function may exhibit similarities between instruments of identical design, but will vary between individual instruments and with drift over time, and therefore must be accounted for by routine calibrations.[27–29] The remaining parameters are combined, and, typically in ratio to the value of a reference peak intensity (such as the carbon 1s peak), form the so-called RSFs.

To account for the depth of emission due to inelastic scattering, both the well-known TPP-2M[30] and Seah's universal curve equations[4,31] may be used to estimate IMFPs and effective attenuation lengths (EALs). These two methods have been found to be valid within the ranges of 50 to 200 keV[32] and 100 to 30 keV,[4,31] respectively, and are therefore suitable for HAXPES applications. There are also several databases available from which values for both EALs and IMFPs may be obtained.[33,34]

The effects of elastic scattering are most significant in materials consisting of heavy elements, particularly at lower electron kinetic energies. At higher kinetic energies, the effects of elastic scattering are negligible in materials that comprise light elements such as organic matter. When elastic scattering must be considered, the change in observed electron intensity may be estimated using the appropriate EALs in place of the inelastic mean free path in Equation 1. The works of Jablonski and Powell[35–38] provide detailed insight into the effects of elastic scattering on photoelectron intensity, methods for their correction and the various types of EAL that should be used. Care must be taken that the appropriate combinations of terms for elastic and inelastic scattering are used when calculating RSFs to avoid redundancies, that is, if appropriate EALs are used, the term S in Equation 1 is not required and vice versa.

Apart from electron transport and instrumental considerations, the remaining components of Equation 1 are those relating to the photoemission event itself: the photoionisation cross sections and asymmetry parameters. Typically, an analyst working without a ready-made set of RSFs will need to obtain values for these parameters from the many available databases,[33,39–43] and interpolate and combine these appropriately in order to calculate compositions from measured photoemission peak intensities.

The angular anisotropy of photoelectron emission, represented by F in Equation 1, may be reasonably accounted for within the dipole approximation at traditional photon energies[40,41]; this is encapsulated by the term β. However, at higher energies, quadrupole and higher order contributions may become significant. At these higher energies, photoelectron angular distributions have been approximated by the introduction of two nondipole terms δ and γ in Equation 2 for linearly polarised light, and Equation 3 for unpolarised light.[44] For the case of part-polarisation, an expression may also be formed by the combination of linearly polarised components at different angles in appropriate proportion, as given in Equation 4.* An alternative form for the part-polarised equation, expressed in terms of angles more appropriate for describing instrument geometry, has been previously published by Shard and Reed[45]:

$$F_L = \frac{\beta}{2}\left(3\cos^2\theta - 1\right) + \left(\delta + \gamma\cos^2\theta\right)\sin\theta\cos\phi \tag{2}$$

$$F_U = \frac{\beta}{4}\left(3\cos^2\omega - 1\right) + \left(\delta + \frac{\gamma}{2}\sin^2\omega\right)\cos\omega \tag{3}$$

$$F_P = P\left(1 + \frac{\beta}{2}\left(3\cos^2\theta - 1\right) + \left(\delta + \gamma\cos^2\theta\right)\sin\theta\cos\phi\right) + (1-P)\left(1 + \frac{\beta}{2}\left(3\sin^2\theta\sin^2\phi - 1\right) + \left(\delta + \gamma\sin^2\theta\sin^2\phi\right)\sin\theta\cos\phi\right) \tag{4}$$

where F_L denotes the angular anisotropy term for linearly polarised light; F_U denotes the angular anisotropy term for unpolarised light; F_P denotes the angular anisotropy term for part-polarised light; β is the dipole asymmetry parameter; δ and γ are the nondipolar asymmetry parameters; θ is the angle between the photoelectron emission vector and the polarisation direction; ϕ is the angle between the direction of photon flux and the projection of the photoelectron emission vector onto the plane perpendicular to the polarisation direction; P is the degree of polarisation, where a value of 1 or 0 is equivalent to full linear polarisation, and 0.5 is equivalent to unpolarised light; and ω is the angle between the direction of photon flux and photoelectron emission vector.

The angles θ, ϕ and ω are illustrated in Figure 1.

A practical set of RSFs may therefore be obtained by cross-referencing multiple databases for each of these parameters for a given photon energy and combining with database or formula-determined values for the electron transport parameters.[10,14] This is often inconvenient, time consuming, and, depending on the instrument and database, may require some interpolation.

The use of descriptive formulae for all relevant parameters is of practical value for RSF calculation, through which an entire set of RSFs can be determined simply by entering the photon energy and geometry of the instrument to be used. To facilitate this, we have developed the descriptive formulae described in Section 4 for core-level photoemission cross sections and asymmetry parameters, based upon fitting of database values in the 1.5- to 10-keV photon energy range.

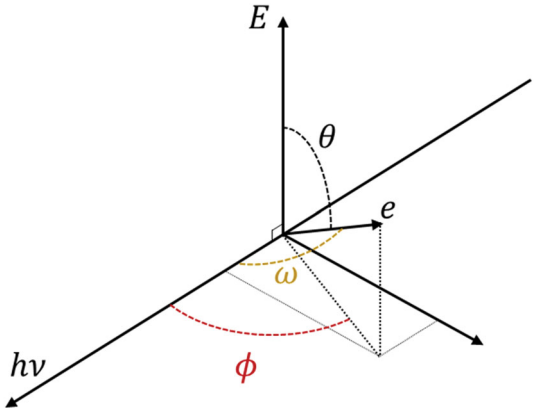

FIGURE 1 Diagram illustrating the angles involved in the calculation of asymmetry effects, where *hν* denotes the direction of photon flux, *E* denotes the direction of polarisation, *e* denotes the direction of photoemission, and θ, ϕ and ω refer to the angles defined in Equations 2 and 3 for anisotropic emission of electrons

3 | SOURCES OF DATA

There are several databases of cross section and asymmetry parameter values available[39–43] across a range of atomic numbers, photon energies and methods of calculation. The cross sections calculated by Scofield[39] are frequently used to determine sensitivity factors, and recent digitisation work has made these, and other sources, more readily available.[46–48]

The differences between cross-section data sources are important to consider when developing sensitivity factors, because this variation provides insight into the accuracy of the photoionisation cross sections and, therefore, the resulting RSFs. Here, we have considered the variation between three well-known databases: those of Scofield,[39] Trzhaskovskaya and Yarzhemsky,[40,41] and Sabbatucci and Salvat.[43] In cases where these databases share entries for a given atomic number, subshell and photon energy (±50 eV), the average was taken, and the values were compared to assess the variability. The relative differences between each database and the average values are plotted in Figure 2 in order to illustrate the variation.

The variation between these databases is typically within ±10%, and no more than ±15% from the mean within the subset of values selected here. Across all the selected values, the standard deviation from the mean is less than 5% for all three databases. A significant contributor to this deviation arises from the Scofield database cross sections that are on average higher than the others—whereas the more recently calculated cross sections are in closer agreement, the popularity of Scofield's original database makes it important to consider when evaluating the variation. When comparing the databases directly with each other, the standard deviations between the databases across the sampled points are approximately 6% between Trzhaskovskaya and Yarzhemsky[40,41] and Scofield,[39] 7% between Sabbatucci and Salvat[43] and Scofield,[39] and 2% between Sabbatucci and Salvat[43] and Trzhaskovskaya and Yarzhemsky.[40,41]

For the purposes of fitting the cross-section values to generate the formulae described in Section 4, the database produced by Sabbatucci and Salvat[43] was used, which provides an appropriately fine energy mesh across the range of interest.

Photoemission asymmetry parameters were modelled from the works of Trzhaskovskaya et al,[40,41,49] which provide an appropriate and useful database. In fact, there are no other complete, readily accessible databases of these parameters currently available.

4 | PREDICTIVE EQUATIONS

Empirical fitting of the photoionisation cross sections, σ; the dipole asymmetry parameter, β; and the nondipolar asymmetry parameters δ and γ was performed across the range of photon energies from 1–10 keV and across all elements from $Z = 3$ to $Z = 98$. Fitting was performed by inspection using empirical expressions. For each subshell, it was possible to find predictive equations that accurately describe the photoionisation parameters using inputs of only the photon energy and atomic number. Parameters within the equations were varied to obtain the best fit using least-squares fitting in Microsoft Excel 365, using the 'Solver' add-on. Initial approximate values were selected manually to match the general form of the data, followed by optimisation using the generalised reduced gradient nonlinear method. The resulting fits obtained for these parameters are given by Equations A1 to A36 in the appendix, together with their tabulated coefficients for each subshell. Subshells with binding energy less than 50 eV were not included to avoid undue complexity in the equations developed and because these peaks are rarely used in XPS quantification. It should be noted that for the asymmetry parameters, β and γ, the descriptive equations have a different form for the *s* subshells. A spreadsheet implementing these equations, and utilising IMFPs calculated by the method of Seah,[4] is provided in the

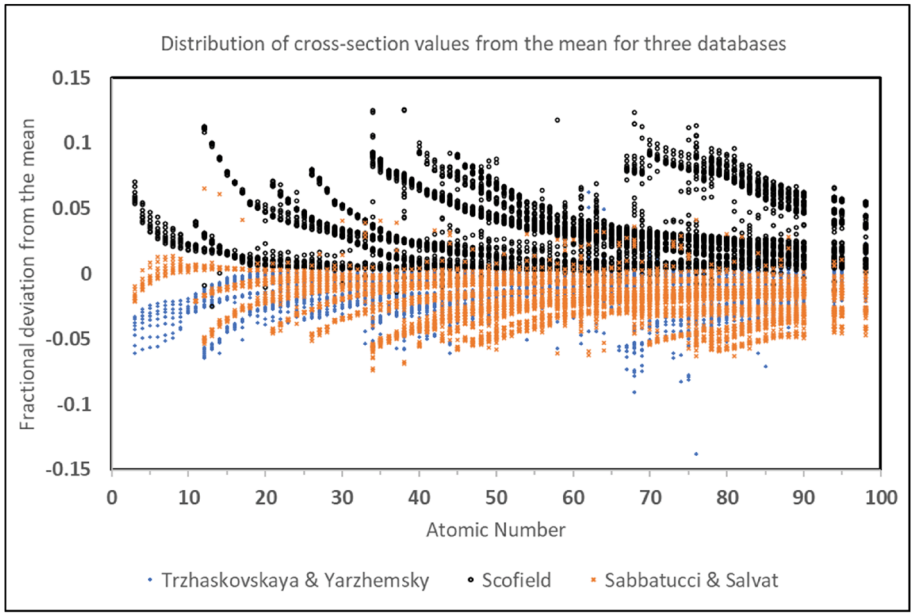

FIGURE 2 A sample of cross sections from three database sources, plotted as the fractional difference of each from the mean of all three. Cross sections are plotted for photon energies from 1500 to 10,000 eV, for photon energies present in all databases (within 50 eV)

supporting information; this may be used to determine estimated RSFs for any entered geometry and photon energy.

4.1 | Fitting error

Figure 3 depicts the fractional deviation of the modelled photoionisation cross sections compared with the full set of database values used from Sabbatucci and Salvat.[43] For elements with atomic number less than 83, the maximum variation is less than 13%, with a root-mean-square (RMS) deviation of 1.5%. This is less than the deviation between the cross-section databases described in Section 3 and significantly less than the potential uncertainties associated with peak area quantification.[22] However for very high atomic number ($Z > 90$), the deviation of the fit can become unacceptable, in particular for the extremes of the fit, such as in the case of the 5s subshell, highlighted in red in Figure 3, for which the fractional deviation reaches almost 60% at $Z = 98$. Despite these extreme outliers, the RMS deviation from the database values across the entire dataset is only 3.5%, and the method thus creates a satisfactory RSF library for use in quantification. In the RSF generation spreadsheet provided in the supporting information, specific subshells that have a potential deviation of greater than 15% for any photon energy in the 1.5–10 keV range are excluded.

It is also useful to consider the behaviour of specific, commonly measured photoelectron peaks. Cross sections approximately follow a power-law with increasing photon energy. The exponent varies for different subshells. Figure 4 depicts the modelled photoionisation cross sections of the C 1s; Au 4s and $4f_{7/2}$; Ag $3d_{5/2}$ and Si 1s and $2p_{3/2}$ with photon energy. For all of these subshells, the model shows excellent agreement with database values.

Notably, cross sections and derived RSFs may also inform experimental decisions prior to analysis—for example, at higher photon energies analysts may consider using alternative subshells from gold

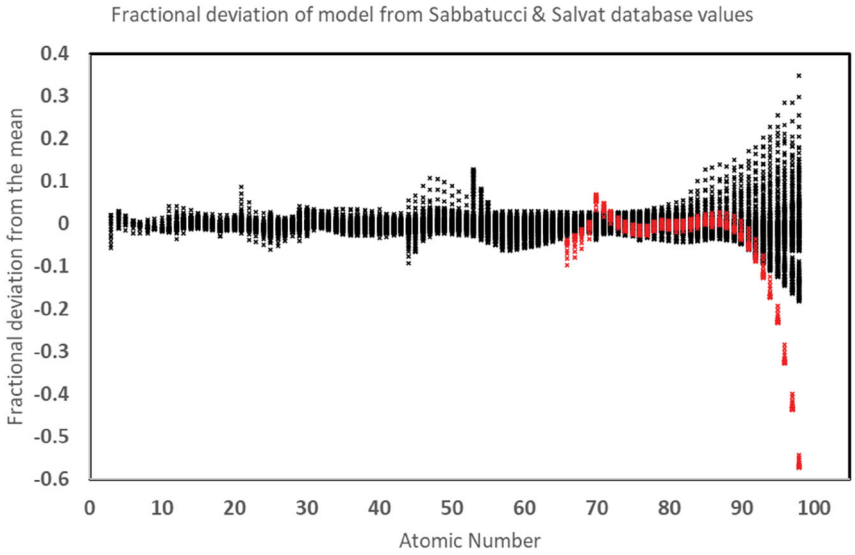

FIGURE 3 Fractional deviation between modelled cross-section values and the Sabbatucci and Salvat[43] database values. The most extreme deviation is observed for very high atomic number elements, in particular for the 5s subshell (highlighted in red) of elements above $Z = 90$

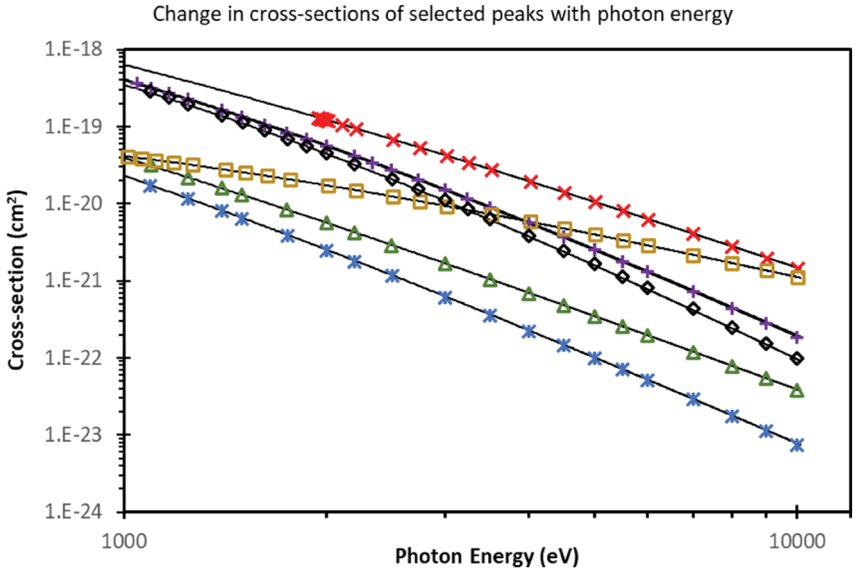

FIGURE 4 Cross-section values from Sabbatucci and Salvat[43] for some selected subshells, along with the associated model (lines), depicted on a log–log plot. Values from the database are shown as points, and the descriptive curves in this paper are shown as lines. Markers correspond to subshells as follows: (Δ, C 1s); (×, Si 1s); (*, Si $2p_{3/2}$); (+, Ag $3d_{5/2}$); (□, Au 4s); (◇, Au $4f_{7/2}$)

as the primary peak for quantification, rather than the 4f peaks commonly used at lower X-ray energy, because these decrease in intensity rapidly with increasing photon energy. Likewise, additional core levels may also be accessed at higher photon energies, which may be preferable for analysis, such as silicon 1s beyond ~2 keV. Figures S1–S3 show database values from Trzhaskovskaya and Yarzhemsky[40,41] for the β, γ and δ asymmetry parameters together with the associated modelled data for selected subshells of interest.

To express errors in fitting for the asymmetry parameters, it is more convenient to consider the absolute error of the modelled values from the database, rather than the fractional error. This is due to the limited range of potential values, and the large number of values that are close to zero, for which the use of the fractional error could cause negligible errors to become dominant. These are plotted for β, γ and δ in Figures S4–S6. Although there are some extreme deviations, the RMS errors for each of these data sets are 0.007, 0.026 and 0.005 for β, γ and δ, respectively.

5 | EXECUTION

By calculating values for the cross sections and asymmetry parameters, and combining with appropriate values for the IMFP and any necessary corrections for elastic scattering, it is possible to generate a complete set of theoretical RSFs for any given instrument geometry and photon energy. In order to minimise the tedious and error-prone process of replicating these formulae individually, a spreadsheet performing these calculations, and using Seah's method for calculation of the IMFP,[31] is provided in the supporting information.

In order to use the spreadsheet, the instrument geometry, photon energy, the degree of polarisation and a specific subshell for all RSFs to be normalised to may be entered into the 'Control' sheet. The spreadsheet may then be used to output an RSF database in the sheet 'RSFs'. For basic use, this is all that is required, and all other sheets are locked to prevent errors. An optional flat multiplier for the angular anisotropy term may also be applied (labelled 's', as per Equation 1) in order to adjust for elastic scattering effects. Typical values for this parameter are between 0.5 and 1, and relationships to the single scattering albedo can be found elsewhere.[32,50] All generated RSFs should only be used in conjunction with those from the same calculation—if any parameters are changed, the resulting RSFs are no longer comparable with any that were previously determined.

A selection of example RSF databases that correspond to commercial instrument geometries have been generated using this spreadsheet and are also provided in the supporting information. Examples of data sets analysed using RSF's calculated in a similar fashion for silver and gallium source instruments can be found in previous work[10,14] and provide results that are reasonable consistent with expected compositions. Notably, the RSF values determined here differ slightly from those previously calculated,[10,14] with an RMS deviation of 24% for the silver-source instrument, and 10% for the liquid-gallium-source instrument. This is due to a combination of differences in the estimation method for the cross sections, the calculated effects of angular anisotropy and the calculation of the IMFP. These refinements represent improvements over the previously published RSFs.

For advanced use, should the user wish to replace the IMFPs used with an alternative source, or to apply corrections for elastic scattering effects, instructions for unlocking the relevant sheets are detailed.

6 | CONCLUSIONS

Here, we have developed a practical route for new HAXPES users to generate libraries of RSFs through the provision of descriptive formulae to estimate photoionisation cross sections and asymmetry parameters for X-ray sources in the range 1.5 to 10 keV. The error in these formulae is similar to the difference between different databases and significantly lower than other typical uncertainties in the quantification of peak intensities from X-ray photoelectron spectra, such as the estimation of peak areas and electron attenuation lengths.[4,22] Although somewhat large and complex in form, the formulae obtained are straightforward to implement, and a spreadsheet has been provided in the supporting information to enable their application in combination with estimated IMFPs to generate an RSF library for a given photon energy and instrument geometry. Example RSF databases have also been provided for a number of commercial instrument geometries.

ACKNOWLEDGEMENTS

The work was funded by the UK Department of Business, Energy, and Industrial Strategy through the National Measurement System programme (projects NMS/ST20-21). This work was supported by the Henry Royce Institute, funded through EPSRC Grants EP/R00661X/1, EP/P025021/1 and EP/P025498/1.

AUTHOR CONTRIBUTIONS

The manuscript was written through contributions of all authors. D.J.H.C. and A.G.S. determined the fit equations and performed the fitting. D.J.H.C. designed the RSF generation spreadsheet. B.F.S. and W.R.F. reviewed the manuscript and the spreadsheet.

DATA AVAILABILITY STATEMENT

The data associated with this paper are openly available from https://www.npl.co.uk/research/surface-technology/xpsamrsf.

ORCID

David J. H. Cant https://orcid.org/0000-0002-4247-5739
Alexander G. Shard https://orcid.org/0000-0002-8931-5740

ENDNOTE

* It should be noted that a different expression for the part-polarised case has been published by Nefedov and Nefedova,[44] which does not consistently agree with the linear and unpolarised equations at the corresponding values of the polarisation factor.

REFERENCES

1. Seah MP. A system for the intensity calibration of electron spectrometers. *J Electron Spectros Relat Phenomena*. 1995;71(3):191-204. doi:10.1016/0368-2048(94)02275-5
2. Seah MP, Gilmore IS, Spencer SJ. Quantitative XPS: I. Analysis of X-ray photoelectron intensities from elemental data in a digital photoelectron database. *J Electron Spectros Relat Phenomena*. 2001;120(1-3):93-111. doi:10.1016/S0368-2048(01)00311-5
3. Jablonski A, Powell CJ. Practical expressions for the mean escape depth, the information depth, and the effective attenuation length in Auger-electron spectroscopy and x-ray photoelectron spectroscopy. *J Vac Sci Technol A*. 2009;27(2):253-261. doi:10.1116/1.3071947
4. Seah MP. Simple universal curve for the energy-dependent electron attenuation length for all materials. *Surf Interface Anal*. 2012;44(10):1353-1359. doi:10.1002/sia.5033
5. Powell CJ, Jablonski A. Surface sensitivity of X-ray photoelectron spectroscopy. *Nucl Instruments Methods Phys Res Sect A Accel Spectrometers, Detect Assoc Equip*. 2009;601(1-2):54-65. doi:10.1016/j.nima.2008.12.103
6. Seah MP, Gilmore IS, Spencer SJ. Quantitative AES IX and quantitative XPS II: Auger and x-ray photoelectron intensities and sensitivity factors from spectral digital databases reanalysed using a REELS database. *Surf Interface Anal*. 2001;31(8):778-795. doi:10.1002/SIA.1109
7. Seah MP, Gilmore IS. Quantitative x-ray photoelectron spectroscopy: quadrupole effects, shake-up, Shirley background, and relative sensitivity factors from a database of true x-ray photoelectron spectra. *Phys Rev B*. 2006;73(17):174113. doi:10.1103/PhysRevB.73.174113
8. Seah MP, Gilmore IS. Erratum: quantitative x-ray photoelectron spectroscopy: quadrupole effects, shake-up, Shirley background, and relative sensitivity factors from a database of true x-ray photoelectron spectra [Phys. Rev. B **73**, 174113 (2006)]. *Phys Rev B*. 2007;75(14):149901. doi:10.1103/PhysRevB.75.149901
9. Wagner CD. X-ray photoelectron spectroscopy with x-ray photons of higher energy. *J Vac Sci Technol A*. 1998;15(2):518-523. doi:10.1116/1.569459
10. Shard AG, Counsell JDP, Cant DJH, et al. Intensity calibration and sensitivity factors for XPS instruments with monochromatic Ag Lα and Al Kα sources. *Surf Interface Anal*. 2019;51(7):763-773. doi:10.1002/sia.6647
11. Siol S, Mann J, Newman J, et al. Concepts for chemical state analysis at constant probing depth by lab-based XPS/HAXPES combining soft and hard X-ray sources. *Surf Interface Anal*. 2020;52(12):802-810. doi:10.1002/sia.6790
12. Weiland C, Rumaiz AK, Pianetta P, Woicik JC. Recent applications of hard x-ray photoelectron spectroscopy. *J Vac Sci Technol A*. 2016;34(3):030801. doi:10.1116/1.4946046
13. Otendal M, Tuohimaa T, Vogt U, Hertz HM. A 9keV electron-impact liquid-gallium-jet x-ray source. *Rev Sci Instrum*. 2008;79(1):016102. doi:10.1063/1.2833838
14. Spencer BF, Maniyarasu S, Reed BP, et al. Inelastic background modelling applied to hard X-ray photoelectron spectroscopy of deeply buried layers: a comparison of synchrotron and lab-based (9.25 keV) measurements. *Appl Surf Sci*. 2021;541:148635. doi:10.1016/j.apsusc.2020.148635
15. Maniyarasu S, Ke JC-R, Spencer BF, Walton AS, Thomas AG, Flavell WR. Role of alkali cations in stabilizing mixed-cation perovskites to thermal stress and moisture conditions. *ACS Appl Mater Interfaces*. 2021;13(36):43573–43586. doi:10.1021/ACSAMI.1C10420.
16. Mallinson CF, Yates PM, Mack P, Watts JF. XPS examination of the native oxide layer on Kovar using aluminium, magnesium and silver x-ray sources. *Surf Sci Spectra*. 2016;23(1):40-50. doi:10.1116/1.4954179
17. Bouttemy M, Béchu S, Spencer BF, Dally P, Chapon P, Etcheberry A. Combined pulsed RF GD-OES and HAXPES for quantified depth profiling through coatings. *Coatings*. 2021;11(6):702. doi:10.3390/COATINGS11060702
18. Risterucci P, Renault O, Zborowski C, et al. Effective inelastic scattering cross-sections for background analysis in HAXPES of deeply buried layers. *Appl Surf Sci*. 2017;402:78-85. doi:10.1016/J.APSUSC.2017.01.046
19. Risterucci P, Renault O, Martinez E, et al. Inelastic background analysis of HAXPES spectra: towards enhanced bulk sensitivity in photoemission. *Surf Interface Anal*. 2014;46(10-11):906-910. doi:10.1002/SIA.5484
20. Zborowski C, Renault O, Torres A, Yamashita Y, Grenet G, Tougaard S. Determination of the input parameters for inelastic background analysis combined with HAXPES using a reference sample. *Appl Surf Sci*. 2018;432:60-70. doi:10.1016/J.APSUSC.2017.06.081
21. Baer DR, McGuire GE, Artyushkova K, Easton CD, Engelhard MH, Shard AG. Introduction to topical collection: reproducibility challenges and solutions with a focus on guides to XPS analysis. *J Vac Sci Technol A*. 2021;39(2):021601. doi:10.1116/6.0000873
22. Shard AG. Practical guides for x-ray photoelectron spectroscopy: quantitative XPS. *J Vac Sci Technol A*. 2020;38(4):041201. doi:10.1116/1.5141395
23. Brundle CR, Crist BV, Bagus PS. Accuracy limitations for composition analysis by XPS using relative peak intensities: LiF as an example. *J Vac Sci Technol A*. 2021;39(1):013202. doi:10.1116/6.0000674
24. Brundle CR, Crist BV. X-ray photoelectron spectroscopy: a perspective on quantitation accuracy for composition analysis of homogeneous materials. *J Vac Sci Technol A*. 2020;38(4):041001. doi:10.1116/1.5143897
25. Yasuno S, Oji H, Watanabe Y, Hirosawa I. Relative sensitivity factors for hard X-ray photoelectron spectroscopy with photon energies of 3.0, 5.9, 7.9, and 9.9 keV. *Surf Interface Anal*. 2020;52(12):869-874. doi:10.1002/SIA.6855
26. Powell CJ. Practical guide for inelastic mean free paths, effective attenuation lengths, mean escape depths, and information depths in x-ray photoelectron spectroscopy. *J Vac Sci Technol A*. 2020;38(2):023209. doi:10.1116/1.5141079
27. Seah MP. XPS reference procedure for the accurate intensity calibration of electron spectrometers? Results of a BCR intercomparison co-sponsored by the VAMAS SCA TWA. *Surf Interface Anal*. 1993;20(3):243-266. doi:10.1002/sia.740200309
28. Shard AG, Spencer SJ. Intensity calibration for monochromated Al Kα XPS instruments using polyethylene. *Surf Interface Anal*. 2019;51(6):618-626. doi:10.1002/sia.6627
29. Reed BP, Cant DJH, Spencer SJ, et al. Versailles project on advanced materials and standards interlaboratory study on intensity calibration for x-ray photoelectron spectroscopy instruments using low-density polyethylene. *J Vac Sci Technol A*. 2020;38(6):063208. doi:10.1116/6.0000577
30. Tanuma S, Powell CJ, Penn DR. Calculations of electron inelastic mean free paths. V. Data for 14 organic compounds over the 50-2000 eV range. *Surf Interface Anal*. 1994;21(3):165-176. doi:10.1002/sia.740210302
31. Seah MP. An accurate and simple universal curve for the energy-dependent electron inelastic mean free path. *Surf Interface Anal*. 2012;44(4):497-503. doi:10.1002/SIA.4816
32. Jablonski A, Powell CJ. Effective attenuation lengths for different quantitative applications of X-ray photoelectron spectroscopy. *J Phys Chem Ref Data*. 2020;49(3):033102. doi:10.1063/5.0008576
33. Powell CJ. A new NIST database for the simulation of electron spectra for surface analysis (SESSA): application to angle-resolved X-ray photoelectron spectroscopy of HfO2, ZrO2, HfSiO4, and ZrSiO4 films on silicon. *AIP Conference Proceedings*. 2005;788(107):107-111. doi:10.1063/1.2062946

34. "NIST standard reference database 82|NIST electron effective-attenuation-length database," 2009. https://www.nist.gov/srd/nist-standard-reference-database-82 (Accessed Aug 23, 2021).
35. Powell CJ, Jablonski A. Influence of elastic-electron scattering on measurements of silicon dioxide film thicknesses by x-ray photoelectron spectroscopy. *J Vac Sci Technol A*. 2001;19(5):2604-2611. doi:10.1116/1.1397463
36. Jablonski A, Powell CJ. Effective attenuation lengths for photoelectrons emitted by high-energy laboratory X-ray sources. *J Electron Spectros Relat Phenomena*. 2015;199:27-37. doi:10.1016/j.elspec.2014.12.011
37. Jablonski A, Powell CJ. Effective attenuation lengths for quantitative determination of surface composition by Auger-electron spectroscopy and X-ray photoelectron spectroscopy. *J Electron Spectros Relat Phenomena*. 2017;218:1-12. doi:10.1016/j.elspec.2017.04.008
38. Jablonski A. Parameterization of HAXPES photoelectrons with kinetic energies up to 10 keV. *Appl Surf Sci*. 2015;346:503-519. doi:10.1016/J.APSUSC.2015.04.028
39. Scofield J. H., "Theoretical photoionization cross sections from 1 to 1500 keV," U.S. Atomic Energy Commission, 1973. 10.2172/4545040.
40. Trzhaskovskaya MB, Yarzhemsky VG. Dirac–Fock photoionization parameters for HAXPES applications. *At Data Nucl Data Tables*. 2018;119:99-174. doi:10.1016/J.ADT.2017.04.003
41. Trzhaskovskaya MB, Yarzhemsky VG. Dirac–Fock photoionization parameters for HAXPES applications, part II: inner atomic shells. *At Data Nucl Data Tables*. 2019;129–130:101280. doi:10.1016/J.ADT.2019.05.001
42. Yeh JJ, Lindau I. Atomic subshell photoionization cross sections and asymmetry parameters: 1 ≤ Z ≤ 103. *At Data Nucl Data Tables*. 1985;32(1):1-155. doi:10.1016/0092-640X(85)90016-6
43. Sabbatucci L, Salvat F. Theory and calculation of the atomic photoeffect. *Radiat Phys Chem*. 2016;121:122-140. doi:10.1016/J.RADPHYSCHEM.2015.10.021
44. Nefedov VI, Nefedova IS. Angular distribution of the photoelectrons from solids with account for elastic scattering and non-dipolar transitions. *J Electron Spectros Relat Phenomena*. 2000;107(2):131-137. doi:10.1016/S0368-2048(00)00095-5
45. Shard AG, Reed BP. Al Kα XPS reference spectra of polyethylene for all instrument geometries. *J Vac Sci Technol A*. 2020;38(6):063209. doi:10.1116/6.0000578
46. Kalha C, Fernando NK, Regoutz A. Digitisation of Scofield photoionisation cross section tabulated data 2020.
47. Willis J, Kalha C, Trzhaskovskaya MB, Yarzhemsky VG, Scanlon D, Regoutz A. "Digitisation of Trzhaskovskaya Dirac-Fock photoionisation parameters for HAXPES applications." figshare, 2020. doi:10.6084/m9.figshare.13292144.v1
48. Kalha C. et al., "Digitisation of Yeh and Lindau photoionisation cross section tabulated data." https://figshare.com/articles/dataset/Digitisation_of_Yeh_and_Lindau_Photoionisation_Cross_Section_Tabulated_Data/12389750/2 (Accessed Aug. 19, 2021).
49. Trzhaskovskaya MB, Nefedov VI, Yarzhemsky VG. Photoelectron angular distribution parameters for elements Z=1 TO Z=54 in the photoelectron energy range 100–5000 eV. *At Data Nucl Data Tables*. 2001;77(1):97-159. doi:10.1006/adnd.2000.0849
50. Jablonski A, Powell CJ. Improved analytical formulae for correcting elastic-scattering effects in X-ray photoelectron spectroscopy. *Surf Sci*. 2010;604(3-4):327-336. doi:10.1016/J.SUSC.2009.11.025

SUPPORTING INFORMATION

Additional supporting information may be found in the online version of the article at the publisher's website.

How to cite this article: Cant DJH, Spencer BF, Flavell WR, Shard AG. Quantification of hard X-ray photoelectron spectroscopy: Calculating relative sensitivity factors for 1.5- to 10-keV photons in any instrument geometry. *Surf Interface Anal*. 2022;54(4):442-454. doi:10.1002/sia.7059

APPENDIX A: EQUATIONS AND COEFFICIENT TABLES

Here are the final fitted equations for σ, β, γ and δ and associated coefficients corresponding to each subshell. Within the supporting information, a spreadsheet implementation of these can be found, along with some example RSF databases for commercial instrument setups.

A.1 | Cross section

$$\sigma = (a_\sigma + m_\sigma Z) * \left(E_{h\nu} + b_\sigma + n_\sigma Z + (p_\sigma Z)^2\right)^{\left(q_\sigma + r_\sigma e^{\left(-\left\{\frac{Z}{s_\sigma}\right\}^{t_\sigma}\right)}\right)} \quad \text{(A1)}$$

Shell	Cross-section equation coefficients								
	Constant factor, a_σ	Linear multiplier, m_σ	Base constant, b_σ	Base Z multiplier, n_σ	Base Z^2 multiplier, p_σ	Power constant, q_σ	Power multiplier, r_σ	Power exponent denominator, s_σ	Power exponent power, t_σ
1s	−1.63E-10	1.07E-10	2.42E+02	−1.14E+01	1.17E+00	−2.37E+00	−2.63E+00	4.88E+00	3.62E-01
2s	−2.66E-11	4.30E-12	9.08E+01	1.07E+01	8.79E-01	−2.28E+00	−2.14E+00	7.42E+00	3.78E-01
3s	2.76E-12	−1.61E-14	6.42E+02	−1.48E+01	6.05E-01	−1.82E+00	−1.76E+00	3.14E+01	6.52E-01
4s	−1.02E-13	4.61E-15	1.26E+03	−3.90E+01	6.61E-01	−1.97E+00	−1.43E+00	1.64E+01	6.14E-01
5s	9.46E-14	−9.44E-16	8.87E+02	−5.51E+00	−4.97E-02	−1.49E+00	−7.56E-01	9.62E+01	4.52E+00
2p1	−1.27E-08	1.70E-09	2.74E+02	−3.46E+00	6.46E-01	−2.42E+00	−5.82E+00	3.80E+00	2.61E-01
2p3	−2.87E-08	3.76E-09	1.91E+02	4.87E+00	4.61E-01	−2.64E+00	−5.47E+00	3.37E+00	2.85E-01
3p1	9.83E-10	7.18E-11	8.73E+02	−3.31E+01	9.51E-01	−2.70E+00	−2.00E+00	2.92E+01	7.78E-01
3p3	5.22E-09	6.28E-11	3.51E+02	5.98E-01	5.94E-01	−2.52E+00	−6.45E+00	4.42E+00	3.48E-01
4p1	−1.02E−10	3.69E-12	3.08E+03	−1.03E+02	1.10E+00	2.10E-01	−9.01E+00	3.05E+01	1.18E-01
4p3	−1.05E-10	2.89E-12	−1.64E+02	1.20E+01	3.08E-01	7.94E-01	−7.06E+00	2.10E+03	1.02E-01
5p1	7.97E-14	3.79E-15	1.29E+03	−3.33E+01	6.30E-01	−1.97E+00	−2.12E+00	4.21E+01	1.01E+00
5p3	−6.01E-13	2.91E-14	2.30E+03	−3.96E+01	5.13E-01	−2.01E+00	−1.67E+00	5.45E+01	9.84E-01
3d3	−2.10E-06	8.48E-08	9.90E+01	5.18E+00	3.36E-01	−2.96E+00	−7.90E+00	4.55E+00	3.00E-01
3d5	−3.90E-06	1.56E-07	5.37E+01	8.05E+00	2.70E-01	−3.05E+00	−8.49E+00	3.44E+00	2.93E-01
4d3	1.29E-06	−8.41E-09	2.70E+02	5.20E-02	4.84E-01	−1.84E+00	−1.66E+01	2.12E+00	2.20E-01
4d5	1.78E-06	−1.08E-08	3.36E+02	5.21E-02	4.52E-01	−1.68E+00	−1.70E+01	1.69E+00	1.99E-01
4f5	−3.48E-05	1.20E-06	1.01E+02	3.79E+00	2.23E-01	−4.09E+00	−2.17E+04	2.88E-02	3.03E-01
4f7	−4.39E-05	1.52E-06	1.01E+02	3.74E+00	2.16E-01	−4.09E+00	−2.16E+04	2.87E-02	3.03E-01

A.2 | Beta

$$\beta_S = a_\beta + m_\beta\left(\frac{Z}{100}\right)^{q_\beta} - n_\beta e^{s_\beta\left(\frac{Z}{100}\right)} \tag{A2}$$

$$a_\beta = c_{a\beta} + d_{a\beta}\left(E_{hv}/1000\right) \tag{A3}$$

$$m_\beta = d_{m\beta}\left(E_{hv}/1000\right)^{g_{m\beta}} \tag{A4}$$

$$q_\beta = d_{q\beta}\left(E_{hv}/1000\right)^{g_{q\beta}} \tag{A5}$$

$$n_\beta = d_{n\beta}\left(E_{hv}/1000\right)^{g_{n\beta}} \tag{A6}$$

$$s_\beta = d_{s\beta}\left(E_{hv}/1000\right)^{g_{s\beta}} \tag{A7}$$

$$\beta = a_\beta - m_\beta\left(\frac{Z}{100} - b_\beta\right)^2 * \left(\frac{Z}{100}\right)^{q_\beta} - n_\beta e^{-t_\beta} \tag{A8}$$

$$a_\beta = c_{a\beta} + d_{a\beta}\left(E_{hv}/1000\right) \tag{A9}$$

$$m_\beta = d_{m\beta}\left(E_{hv}/1000\right)^{g_{m\beta}} \tag{A10}$$

$$b_\beta = d_{b\beta}\left(E_{hv}/1000\right)^{g_{b\beta}} \tag{A11}$$

$$q_\beta = d_{q\beta}\left(E_{hv}/1000\right) \tag{A12}$$

$$n_\beta = n_\beta \tag{A13}$$

$$t_\beta = \left(\frac{E_K}{r_\beta}\right)^{s_\beta} \tag{A14}$$

$$s_\beta = c_{s\beta} + \frac{d_{s\beta}}{\left(E_{hv}/1000\right)} \tag{A15}$$

$$r_\beta = c_{r\beta} + d_{r\beta}\left(E_{hv}/1000\right) \tag{A16}$$

	β_S equation coefficients									
Shell	$c_{a\beta}$	$d_{a\beta}$	$d_{m\beta}$	$g_{m\beta}$	$d_{q\beta}$	$g_{q\beta}$	$d_{n\beta}$	$g_{n\beta}$	$d_{s\beta}$	$g_{s\beta}$
1s	2.00E+00	−1.03E-02	6.17E-01	1.58E-01	1.78E+00	2.74E-02	0.00E+00	0.00E+00	0.00E+00	0.00E+00
2s	2.01E+00	−1.04E-02	5.42E-01	1.18E-01	1.59E+00	3.70E-02	6.40E-03	3.40E-02	9.29E+00	−2.04E-01
3s	2.00E+00	−2.73E-02	4.72E-02	9.01E-01	2.39E-01	2.32E-01	1.72E-03	−1.07E-01	6.70E+00	−4.52E-02
4s	1.44E+00	1.89E-02	5.35E-01	−5.01E-02	1.20E-03	2.43E+00	5.87E-05	1.59E+00	1.04E+01	−2.94E-01
5s	1.34E+00	1.61E-02	6.27E-01	−1.92E-02	1.19E-03	2.30E+00	1.41E-04	1.22E+00	8.77E+00	−2.26E-01

	β equation coefficients (part 1)					
Shell	$c_{a\beta}$	$d_{a\beta}$	$d_{m\beta}$	$g_{m\beta}$	$d_{b\beta}$	$g_{b\beta}$
2p1	1.48E+00	−6.67E-03	3.98E+01	−8.14E-01	2.24E-01	4.57E-01
2p3	1.55E+00	0.00E+00	3.49E+01	−7.85E-01	2.37E-01	4.57E-01
3p1	1.64E+00	−4.40E-03	9.59E+00	−5.60E-01	3.56E-01	3.89E-01
3p3	2.21E+00	0.00E+00	5.04E+00	−2.87E-01	4.91E-01	2.88E-01
4p1	1.74E+00	−1.07E-03	3.57E+00	−3.56E-01	4.76E-01	3.48E-01
4p3	1.75E+00	0.00E+00	5.75E+00	−3.87E-01	4.56E-01	3.16E-01
5p1	1.72E+00	−2.35E-03	3.52E+00	−3.54E-01	5.20E-01	3.12E-01
5p3	1.77E+00	0.00E+00	3.25E+00	−1.86E-01	4.57E-01	3.28E-01
3d3	1.32E+00	0.00E+00	6.86E+00	−2.70E-01	4.67E-01	3.40E-01
3d5	1.24E+00	0.00E+00	8.76E+00	−5.74E-01	4.22E-01	4.17E-01
4d3	1.53E+00	0.00E+00	5.81E+00	−3.17E-01	5.28E-01	3.38E-01
4d5	1.41E+00	0.00E+00	4.88E+00	−6.01E-01	5.36E-01	4.09E-01
5d3	1.44E+00	−2.50E-05	4.55E+00	−1.82E-01	6.06E-01	2.73E-01
5d5	1.46E+00	−2.49E-05	2.51E+00	−4.04E-01	6.60E-01	3.50E-01
4f5	1.06E+00	0.00E+00	4.41E+00	−6.23E-01	6.20E-01	3.95E-01
4f7	1.05E+00	−4.43E-06	4.10E+00	−6.43E-01	6.31E-01	3.99E-01

	β equation coefficients (part 2)					
Shell	$d_{q\beta}$	n_β	$c_{s\beta}$	$d_{s\beta}$	$c_{r\beta}$	$d_{r\beta}$
2p1	1.11E-02	1.10E+00	5.01E-01	2.31E-01	5.76E+01	1.75E+01
2p3	1.07E-02	1.31E+00	5.25E-01	3.31E-03	6.09E+01	2.51E+01
3p1	0.00E+00	1.40E+00	6.96E-01	1.35E-01	2.23E+01	7.56E+01
3p3	0.00E+00	2.90E+00	3.72E-01	9.16E-02	7.58E+01	1.37E+02
4p1	0.00E+00	2.01E+00	9.81E-01	0.00E+00	0.00E+00	2.23E+02
4p3	3.03E-04	8.94E-01	1.41E+00	0.00E+00	0.00E+00	2.27E+02
5p1	3.06E-04	7.87E-01	8.11E+00	0.00E+00	0.00E+00	7.37E+02
5p3	3.05E-04	7.83E-01	8.20E+00	0.00E+00	0.00E+00	7.12E+02
3d3	5.21E-02	9.45E-01	1.02E+00	5.28E-01	2.06E+02	2.13E+02
3d5	4.06E-02	7.36E-01	1.03E+00	4.45E-01	2.12E+02	1.34E+02
4d3	5.01E-02	2.34E+00	2.90E-01	6.14E-01	3.44E+02	0.00E+00
4d5	1.92E-02	2.93E+00	3.96E-01	3.12E-01	1.39E+02	0.00E+00
5d3	3.96E-02	3.25E+00	5.67E-01	1.36E-02	1.76E+02	1.35E-03
5d5	1.60E-10	2.92E+00	4.81E-01	0.00E+00	1.30E+02	4.44E-09
4f5	6.37E-02	5.52E+00	3.54E-01	1.46E+00	2.44E+02	0.00E+00
4f7	7.21E-02	5.60E+00	3.26E-01	1.34E+00	2.06E+02	0.00E+00

Shell	γ_s equation coefficients							
	a_γ	b_γ	m_γ	n_γ	q_γ	r_γ	p_γ	s_γ
1s	1.06E+00	4.68E-01	5.09E-01	2.41E+00	1.83E+00	−4.71E-01	2.54E+00	1.62E-01
2s	2.31E+00	4.23E-01	2.21E-01	3.40E+00	3.06E+00	3.90E-03	2.18E+00	5.98E-01
3s	2.58E+00	4.46E-01	2.36E-01	1.78E+00	3.04E+00	3.90E-03	1.16E+00	3.27E-01
4s	1.22E+00	3.39E-01	1.18E-02	2.84E+00	−4.69E-01	1.92E-03	5.53E-01	4.47E-03
5s	1.12E+00	3.20E-01	1.07E-02	3.74E+00	−1.96E+00	9.29E-03	4.33E-01	−2.38E-04

Shell	γ equation coefficients (part 1)						
	$d_{a\gamma}$	$g_{a\gamma}$	$d_{m\gamma}$	$g_{m\gamma}$	$d_{u\gamma}$	$g_{u\gamma}$	$c_{w\gamma}$
2p1	1.42E-03	−1.28E+00	6.23E-02	3.60E-01	3.41E+01	−2.34E-01	4.29E-01
2p3	1.42E-03	−1.28E+00	5.35E-02	3.82E-01	3.12E+01	−2.27E-01	4.41E-01
3p1	2.79E-03	5.93E-01	1.24E-02	4.53E-01	1.76E+02	−3.91E-01	−2.29E-01
3p3	5.94E-03	5.09E-01	7.02E-03	5.21E-01	2.07E+02	−4.13E-01	−1.33E-01
4p1	1.71E-03	6.35E-01	3.64E-03	5.83E-01	1.62E+02	−3.96E-01	−6.99E-02
4p3	1.81E-03	6.34E-01	3.19E-03	6.10E-01	1.22E+02	−3.82E-01	4.91E-01
5p1	1.94E-01	1.66E-01	3.52E-01	9.49E-02	2.26E+01	−1.92E-01	1.36E+00
5p3	2.76E-01	1.61E-01	1.42E-01	1.91E-01	2.81E+01	−2.24E-01	1.47E+00
3d3	4.45E-01	−5.08E-01	1.35E-02	5.14E-01	9.48E+01	−3.70E-01	6.04E+00
3d5	3.63E-01	−8.37E-01	1.63E-02	4.91E-01	9.61E+01	−3.83E-01	6.22E+00
4d3	8.61E+05	−2.10E+00	2.40E-03	6.67E-01	1.18E+02	−3.90E-01	5.81E+00
4d5	8.61E+05	−2.13E+00	2.56E-03	6.59E-01	1.12E+02	−3.97E-01	6.11E+00
5d3	7.98E-04	8.64E-01	1.23E-03	8.14E-01	6.32E+01	−4.01E-01	1.91E+00
5d5	8.98E-04	7.79E-01	1.38E-03	7.36E-01	8.99E+01	−4.33E-01	1.42E+00
4f5	8.38E+05	−2.18E+00	3.19E-03	6.31E-01	8.40E+01	−3.91E-01	5.89E+00
4f7	8.62E+05	−2.10E+00	3.91E-03	6.09E-01	8.54E+01	−3.95E-01	5.88E+00

Shell	γ equation coefficients (part 2)						
	$d_{w\gamma}$	n_γ	$c_{r\gamma}$	$d_{r\gamma}$	p_γ	$c_{s\gamma}$	$d_{s\gamma}$
2p1	−2.82E-05	−8.11E-01	8.98E+02	3.15E-01	−2.06E-01	−3.60E+03	2.40E+00
2p3	−3.20E-05	−8.89E-01	6.79E+02	3.90E-01	−2.08E-01	−3.55E+03	2.37E+00
3p1	1.11E-06	2.40E+00	6.75E+01	1.45E-01	−2.90E+00	1.18E+02	3.73E-02
3p3	−1.46E-05	9.20E-01	8.18E+01	1.70E-01	−1.63E+00	7.67E+01	3.73E-02
4p1	9.50E-06	5.45E+00	−1.12E+02	2.71E-01	−7.62E+00	−3.01E+01	1.74E-01
4p3	−1.60E-05	4.38E+00	1.52E+01	2.71E-01	−5.61E+00	7.64E+01	1.91E-01
5p1	−8.81E-05	9.22E-01	1.51E+03	−1.51E-01	−2.96E+01	1.30E+02	1.09E-01
5p3	−9.26E-05	6.96E-01	1.33E+03	−1.33E-01	−3.85E+01	2.82E+01	2.08E-01
3d3	−7.39E-06	8.41E-01	2.48E+02	4.21E-02	−2.50E-01	3.45E+02	−3.00E-02
3d5	−6.97E-06	5.72E-01	2.49E+02	7.04E-03	−8.86E-03	1.01E+02	−1.01E-02
4d3	−2.18E-06	2.97E+00	−5.22E+02	6.04E-01	−7.01E+00	−1.34E+02	2.42E-01
4d5	−1.26E-05	2.80E+00	−4.92E+02	5.85E-01	−6.82E+00	−1.43E+02	2.31E-01
5d3	2.52E-02	2.20E-01	1.23E+03	−1.19E-01	−1.07E-01	−3.36E+01	4.08E-01
5d5	2.51E-02	2.32E-01	1.22E+03	−1.22E-01	−1.05E-01	−3.36E+01	3.98E-01
4f5	−1.17E-05	2.55E+00	−4.94E+02	7.87E-01	−7.43E+00	−1.22E+02	3.14E-01
4f7	−9.40E-06	3.10E+00	−4.66E+02	7.21E-01	−5.67E+00	−1.22E+02	3.60E-01

Shell	δ equation coefficients (part 1)						
	$c_{a\delta}$	$d_{a\delta}$	$c_{m\delta}$	$d_{m\delta}$	$c_{n\delta}$	$d_{n\delta}$	q_{δ}
1s	0.00E+00	0.00E+00	0.00E+00	0.00E+00	−3.32E+16	−2.38E+17	1.04E+00
2s	0.00E+00	0.00E+00	0.00E+00	0.00E+00	−1.86E-03	4.90E-06	8.67E-01
3s	0.00E+00	0.00E+00	0.00E+00	0.00E+00	−8.97E-04	−3.96E-04	1.05E+00
4s	0.00E+00	0.00E+00	0.00E+00	0.00E+00	−2.30E-02	−7.55E-03	1.82E+00
5s	0.00E+00	0.00E+00	0.00E+00	0.00E+00	−1.47E-02	−9.97E-03	1.85E+00
2p1	5.50E-02	4.27E-02	2.03E-01	−2.85E-03	−2.35E-03	1.35E-02	−2.76E-02
2p3	7.74E-03	3.00E-02	9.23E-03	2.06E-03	5.40E-03	1.53E-02	−3.29E-03
3p1	4.17E-02	1.86E-02	1.34E-01	−3.37E-03	−1.70E-02	1.76E-02	8.29E-03
3p3	3.45E-03	6.14E-03	3.40E-02	−5.28E-03	−4.82E-03	1.91E-02	2.28E-02
4p1	4.18E-03	−1.94E-03	2.44E-02	−2.91E-03	−5.72E-03	1.93E-02	1.94E-02
4p3	1.06E-02	−5.02E-03	4.59E-02	−1.09E-02	−5.26E-03	2.27E-02	2.15E-02
5p1	3.49E-03	−5.39E-03	1.51E-02	−4.56E-03	−4.88E-03	2.18E-02	2.28E-02
5p3	3.39E-03	6.73E-04	1.94E-02	−5.45E-03	−4.82E-03	1.84E-02	2.26E-02
3d3	5.74E-02	4.07E-02	7.16E-02	−5.17E-03	−1.54E-02	3.32E-02	7.46E-02
3d5	1.49E-01	7.38E-02	2.73E-01	−7.57E-03	−4.74E-02	2.20E-02	1.02E-01
4d3	2.85E-02	2.06E-02	7.84E-02	−1.28E-02	2.57E-03	3.91E-02	7.54E-02
4d5	2.11E-02	1.13E-02	8.40E-02	−1.90E-02	2.06E-02	4.02E-02	6.83E-02
5d3	1.74E-02	3.28E-02	6.01E-02	−1.03E-02	2.19E-02	5.70E-02	8.45E-02
5d5	1.99E-02	4.55E-03	6.37E-02	−1.28E-02	1.89E-02	4.95E-02	6.87E-02
4f5	6.41E-02	1.20E-02	5.80E-02	−2.89E-02	4.26E-02	1.18E-01	−1.62E-01
4f7	7.30E-02	1.18E-02	7.41E-02	−2.90E-02	4.07E-02	1.17E-01	−1.65E-01

Shell	δ equation coefficients (part 2)							
	$c_{s\delta}$	$d_{s\delta}$	$c_{p\delta}$	$d_{p\delta}$	$g_{p\delta}$	$c_{t\delta}$	$d_{t\delta}$	u_{δ}
1s	9.04E-02	−1.90E-03	−3.27E-02	2.99E-02	−1.93E-03	9.13E-01	4.35E-01	4.00E-09
2s	2.11E-01	−3.30E-03	−1.43E-02	1.12E-02	−9.10E-04	2.64E-01	1.88E-01	8.73E-03
3s	3.04E-01	−1.01E-02	−3.27E-02	2.99E-02	−1.93E-03	5.18E-01	2.54E-01	1.60E-02
4s	5.20E-01	−1.11E-02	1.08E-02	2.32E-02	−2.18E-03	9.40E-01	1.75E-01	7.13E-02
5s	5.29E-01	−1.20E-02	1.28E-02	2.85E-02	−2.76E-03	1.07E+00	1.56E-01	7.37E-02
2p1	8.30E-02	1.38E-02	7.42E-02	−5.20E-02	4.01E-03	2.49E-01	1.90E-01	2.21E-02
2p3	1.03E-01	1.10E-02	4.91E-01	−3.83E-01	2.90E-02	2.66E-01	2.16E-01	2.05E-02
3p1	1.14E-01	1.42E-02	−1.78E-01	2.87E-01	−2.66E-02	4.94E-01	2.72E-01	3.23E-02
3p3	1.67E-01	7.07E-03	−2.18E-02	1.53E-01	−2.08E-02	5.00E-01	2.89E-01	3.20E-02
4p1	1.66E-01	1.73E-02	−1.56E-02	2.37E-01	−4.82E-02	8.23E-01	2.77E-01	5.02E-02
4p3	1.83E-01	5.48E-03	−3.16E-03	2.24E-01	−4.98E-02	8.65E-01	3.49E-01	8.22E-02
5p1	1.66E-01	1.36E-02	−1.90E-02	5.35E-02	−2.58E-02	7.81E-01	3.08E-01	6.88E-02
5p3	1.29E-01	6.38E-03	−2.21E-02	6.23E-02	−2.30E-02	8.46E-01	3.41E-01	5.85E-02
3d3	2.12E-01	1.02E-02	3.87E-02	−5.82E-02	4.69E-03	5.13E-01	2.92E-01	5.77E-02
3d5	1.02E-01	1.90E-02	4.16E-02	−4.05E-02	2.79E-03	4.97E-01	3.07E-01	4.33E-02
4d3	3.22E-01	1.04E-03	−7.10E-03	2.26E-01	−6.00E-02	8.66E-01	3.47E-01	5.43E-02
4d5	3.55E-01	2.38E-03	−7.11E-03	2.33E-01	−7.79E-02	9.01E-01	3.17E-01	6.97E-02
5d3	2.72E-01	2.06E-03	−7.09E-03	2.96E-01	−1.68E-01	8.40E-01	7.18E-01	7.79E-02
5d5	3.68E-01	3.12E-03	−7.05E-03	2.90E-01	−6.76E-02	1.08E+00	3.01E-01	5.70E-02
4f5	5.89E-01	−5.41E-03	−1.14E-02	−5.30E-02	−6.79E-02	1.07E+00	3.62E-01	1.07E-01
4f7	6.00E-01	−5.79E-03	−1.13E-02	−5.22E-02	−5.62E-02	1.08E+00	2.92E-01	9.21E-02

A.3 | Gamma

$$Z_{adj} = \frac{Z}{a_\gamma * {E_{hv}}^{b_\gamma}} \tag{A17}$$

$$\gamma_S = \left[m_\gamma * \sin\left(n_\gamma * {Z_{adj}}^{p_\gamma} + q_\gamma\right) + s_\gamma * {Z_{adj}}^{p_\gamma} + r_\gamma\right] * \sqrt{E_{hv}} \tag{A18}$$

$$\gamma = a_\gamma + m_\gamma * \sin\left(u_\gamma * \frac{Z}{100} + w_\gamma\right) + n_\gamma * e^{-(r_\gamma)} + p_\gamma * e^{-(s_\gamma)} \tag{A19}$$

$$a_\gamma = d_{a\gamma}(E_{hv})^{g_{a\gamma}} \tag{A20}$$

$$m_\gamma = d_{m\gamma}(E_{hv})^{g_{m\gamma}} \tag{A21}$$

$$u_\gamma = d_{u\gamma}(E_{hv})^{g_{u\gamma}} \tag{A22}$$

$$w_\gamma = c_{w\gamma} + d_{w\gamma}(E_{hv}) \tag{A23}$$

$$n_\gamma = n_\gamma \tag{A24}$$

$$r_\gamma = \frac{E_K}{c_{r\gamma} + d_{r\gamma}(E_{hv})} \tag{A25}$$

$$p_\gamma = p_\gamma \tag{A26}$$

$$s_\gamma = \frac{E_K}{c_{s\gamma} + d_{s\gamma}(E_{hv})} \tag{A27}$$

A.4 | Delta

$$\delta = a_\delta - m_\delta * \left(\frac{Z}{100}\right) + n_\delta \frac{e^{-\left(\frac{\left(\frac{Z}{100} - q_\delta\right)^2}{2{s_\delta}^2}\right)}}{\sqrt{2\pi} * s_\delta} + \frac{p_\delta}{\left(1 + \left[\frac{\frac{Z}{100} - t_\delta}{u_\delta}\right]^2\right)} \tag{A28}$$

$$a_\delta = c_{a\delta} + d_{a\delta}\ln(E_{hv}/1000) \tag{A29}$$

$$m_\delta = c_{m\delta} + d_{m\delta}(E_{hv}/1000) \tag{A30}$$

$$n_\delta = c_{n\delta} + d_{n\delta}(E_{hv}/1000) \tag{A31}$$

$$q_\delta = q_\delta \tag{A32}$$

$$s_\delta = c_{s\delta} + d_{s\delta}(E_{hv}/1000) \tag{A33}$$

$$p_\delta = c_{p\delta} + d_{p\delta}(E_{hv}/1000) + g_{p\delta}(E_{hv}/1000)^2 \tag{A34}$$

$$t_\delta = c_{t\delta} + d_{t\delta}\ln(E_{hv}/1000) \tag{A35}$$

$$u_\delta = u_\delta \tag{A36}$$